Continuum saltation model for sand dunes

Gerd Sauermann,[1,2] Klaus Kroy,[1,*] and Hans J. Herrmann[1,2]
[1]*PMMH, Ecole Supérieure de Physique et Chimie Industrielles (ESPCI), 10, rue Vauquelin, 75231 Paris, Cedex 05, France*
[2]*ICA-1, University of Stuttgart, Pfaffenwaldring 27, 70569 Stuttgart, Germany*
(Received 31 January 2001; published 29 August 2001)

We derive a phenomenological continuum saltation model for aeolian sand transport that can serve as an efficient tool for geomorphological applications. The coupled differential equations for the average density and velocity of sand in the saltation layer reproduce both the known equilibrium relations for the sand flux and the time evolution of the sand flux as predicted by microscopic saltation models. The three phenomenological parameters of the model are a reference height for the grain-air interaction, an effective restitution coefficient for the grain-bed interaction, and a multiplication factor characterizing the chain reaction caused by the impacts leading to a typical time or length scale of the saturation transients. We determine the values of these parameters by comparing our model with wind tunnel measurements. Our main interest are out of equilibrium situations where saturation transients are important, for instance at phase boundaries (ground/sand) or under unsteady wind conditions. We point out that saturation transients are indispensable for a proper description of sand flux over structured terrain, by applying the model to the windward side of an isolated dune, thereby resolving recently reported discrepancies between field measurements and theoretical predictions.

DOI: 10.1103/PhysRevE.64.031305 PACS number(s): 45.70.−n, 92.10.Wa, 92.60.Gn, 92.40.Gc

I. INTRODUCTION

Aeolian sand transport, from the entrainment of single grains to the formation and movement of dunes, have been studied for a long time. One of the most important issues has been the relation $q(u_*)$ between the shear velocity u_* and the saturated sand flux q. The simplest flux law, which gives a cubic relation between shear velocity and sand flux, was already introduced by Bagnold in 1936 [1]. Since that time, many new flux relations have been proposed and used by different authors. The most important improvement was to introduce a threshold to account for the fact that at low wind speeds no sand transport occurs. (An overview of the historical development can be found in Ref. [2].) One of the most widely used flux relations with threshold was proposed by Lettau and Lettau [3]. Analytical derivations of the flux relation starting from a microscopic picture deepened the understanding of the aeolian transport mechanisms a lot [4–7]. An application of sand flux relations is geomorphological problems, where they are used to calculate the erosion rate from the wind shear stress in order to predict the evolution of a free sand surface or dune. However, all flux relations of the type $q(u_*)$ assume that the sand flux is everywhere saturated. This condition is hardly fulfilled at the windward foot of an isolated dune, e.g. a barchan (crescent shaped dune, discussed in Sec. VII), where the bed changes rapidly from bedrock to sand. Correlated measurements of the sand flux and the wind speed performed by Wiggs *et al.* [8] showed a large discrepancy between the measured flux and theoretical predictions of the sand flux using the relation by Lettau and Lettau near the dune's windward foot. Numerical simulations of barchan dunes by Wippermann and Gross [9] that employ this flux law also revealed this problem. Apart from the conditions at the dune's foot, it is conceivable that the sand flux may never reach saturation on the entire windward side of a dune, where the shear velocity increases gradually from the foot to the crest. Such effects are obviously not captured by an equilibrium flux law. To overcome the limitation of the equilibrium relations and to get information about the dynamics of the aeolian sand transport, numerical simulations based on the grain scale have been performed [10–12]. They showed that the typical time to reach the equilibrium state in saltation on a flat surface is approximately two seconds, which was later confirmed by wind tunnel measurements [13]. The problem of simulations on the basis of grains is that they can neither now nor in the near future be used to calculate the evolution of macroscopic geomorphologies.

In the following we derive a dynamic continuum model that allows for saturation transients and can thus be applied to calculate efficiently the erosion in presence of phase boundaries and velocity gradients. In Sec. II we introduce the phenomenology of aeolian sand transport. In Sec. III we develop a continuum model for a thin fluidlike sand layer on an immobile bed including the time dependence of the sand transport and saturation transients. The following sections discuss special cases, where certain restrictions lead to simpler versions of the model. In Sec. IV we discuss the saturated limit of the model and compare it with flux relations and experimental data from the literature. In Sec. V we disregard the spatial dependence of the sand flux and concentrate on the time evolution of the saltation layer. In Sec. VI we present a reduced ''minimal model'' that can easily be applied to geomorphological problems. Finally, we apply this model in Sec. VII to predict the sand flux on the central slice of a barchan dune.

II. SAND TRANSPORT AND SALTATION

Conventionally, according to the degree of detachment of the grains from the ground, different mechanisms of aeolian and transport such as suspension and bed load are distinguished. The bed load can be further divided into saltation and reptation or creep. A detailed overview of this classifi-

*Corresponding author. Email address: kkroy@ph.ed.ac.uk

cation can be found in Ref. [2]. If we consider typical sand storms, when shear velocities are in the range of 0.18 to $0.6\,\mathrm{m\,s^{-1}}$ [2], particles with a maximum diameter of 0.04–0.06 mm can be transported in suspension. The grains of typical dune sand have a diameter of the order of 0.25 mm and are therefore transported via bed load. For this reason we neglect suspension in the following discussion. Furthermore, we do not distinguish between saltation and reptation but consider jumping grains with a mean trajectory length.

The saltation transport can conceptually be divided into four subprocesses. To initiate saltation some grains have to be entrained directly by the air. This will be called direct aerodynamic entrainment. If there is already a sufficiently large amount of grains in the air the direct aerodynamic entrainment is negligible and grains are mainly ejected by impacting grains. The entrained grains are accelerated by the wind along their trajectory mainly by the drag force before they impact onto the bed, again. This is called the splash process, which comprises the complicated interaction between bed and impacting grain and is currently the subject of theoretical and experimental investigations [14,15]. Finally, the momentum transfered from the air to the grains leads in turn to a deceleration of the air. Through this feedback mechanism the saltation dynamics reaches an equilibrium state, characterized by a saturated density ρ_s and an average velocity u_s of the saltating grains.

In the following we develop an effective continuum model in order to calculate the bed-load transport. The variables will be the density ρ and mean velocity u of the grains within a thin surface layer. The closed system of equations will have three phenomenological parameters. The first parameter α models the loss of energy in the splash process and characterizes the grain-bed interaction. It can be thought of as an effective restitution coefficient. The second parameter z_1 is a reference height between the ground and the mean trajectory height and characterizes the air-grain interaction. These two parameters determine the saturated sand flux q_s, whereas the third parameter γ determines the time scale T_s or length scale l_s of the saturation transients.

III. A CONTINUUM MODEL FOR SALTATION

We consider the bed load as a thin fluid-like granular layer on top of an immobile sand bed. This idea was introduced by Bouchaud *et al.* [16] and used in the following to model avalanches on inclined surfaces near the angle of repose [17,18]. This general idea was later also applied to model the formation and propagation of sand ripples [19,20]. To avoid cumbersome notations we restrict ourselves to a two-dimensional description of a slice of a three-dimensional system that is aligned with the wind direction. By this simplification we neglect the lateral transport, caused for instance by gravity or diffusion, which is typically an order of magnitude smaller than the flux in the wind direction. A further simplification [16–18] is obtained by integrating over the vertical coordinate, which leads to scalar functions and equations for the moving layer.

We start the derivation from the mass and momentum conservation in presence of erosion and external forces. Since the saltation layer can exchange grains with the bed, it represents an open system with the erosion rate Γ as a source term,

$$\frac{\partial \rho}{\partial t} + \frac{\partial}{\partial x}(\rho u) = \Gamma. \tag{1}$$

Here, $\rho(x,t)$ and $u(x,t)$ denote the density and velocity of the grains in the saltation layer, respectively. The erosion rate $\Gamma(x,t)$ counts the number of grains per time and area that get mobilized.

The most important forces acting on the grains are the drag force $f_{drag}(x,t)$ when the grains are in the air, which accelerates the grains, and the friction force $f_{bed}(x,t)$ representing the complicated interaction with the bed, which decelerates the grains. Thus, we can write the momentum conservation for the saltation layer as

$$\frac{\partial u}{\partial t} + \left(u \frac{\partial}{\partial x} \right) u = \frac{1}{\rho}(f_{drag} + f_{bed}). \tag{2}$$

Anticipating changes in $\rho(x,t)$ to be slow compared to those in $u(x,t)$, we have adopted an adiabatic approximation and taken ρ out of the derivatives. Additional forces like gravity that might be important on inclined surfaces or diffusion caused by the splash process are neglected here to keep the model as simple as possible, but could easily be added on the right hand side of Eq. (2). In the following sections we derive phenomenological expressions for the erosion rate Γ and the forces f_{drag} and f_{bed}, which will finally lead to a closed model.

A. The atmospheric boundary layer

Sand transport takes place in the turbulent boundary layer of the atmosphere, near the surface. The Navier-Stokes equation $\rho_{air}\partial_t \mathbf{v} + \rho_{air}(\mathbf{v}\cdot\boldsymbol{\nabla})\mathbf{v} = -\boldsymbol{\nabla} p + \boldsymbol{\nabla}\tau$, where $\mathbf{v}$ denotes the wind velocity, ρ_{air} the density of the air, p the pressure, and τ the shear stress of the air, reduces to

$$\frac{\partial \tau}{\partial z} = 0 \quad \text{or} \quad \tau = \text{const}, \tag{3}$$

by making the usual boundary layer approximation, neglecting $\partial/\partial x, \partial/\partial y$ against $\partial/\partial z$ and assuming steady $\partial/\partial t = 0$ and horizontally uniform $(\mathbf{v}\cdot\boldsymbol{\nabla})\mathbf{v} = \mathbf{0}$ flow. At wind velocities for which sand transport is possible, the air flow is highly turbulent. Therefore, we can neglect the bare viscosity of the air and identify τ with the turbulent shear stress. The standard turbulent closure using the mixing length theory models the turbulent shear stress τ,

$$\tau = \rho_{air}\kappa^2 z^2 \left(\frac{\partial v}{\partial z} \right)^2, \tag{4}$$

where $\kappa \approx 0.4$ denotes the von Kármán constant. From equation (4) we obtain by introducing the characteristic shear velocity u_*,

$$\frac{\partial v}{\partial z} = \frac{u_*}{\kappa z} \quad \text{with} \quad u_* = \sqrt{\frac{\tau}{\rho_{air}}}. \tag{5}$$

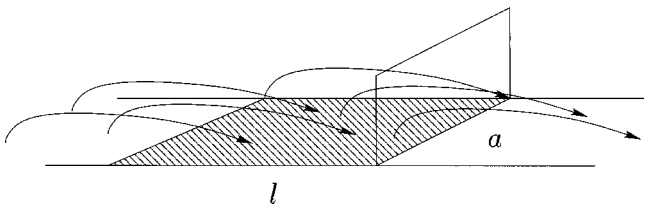

FIG. 1. Sketch of the horizontal sand flux q caused by saltating grains passing the vertical rectangle. The dashed rectangle shows the surface area l times a that is used to calculate the flux Φ of grains impacting onto the surface, where l is the length of the saltation trajectory.

Integration of Eq. (5) leads finally to the well known law of the wall for turbulent flow and therefore to the logarithmic profile of the atmospheric boundary layer

$$v(z)=\frac{u_*}{\kappa}\ln\frac{z}{z_0}, \tag{6}$$

where z_0 denotes the roughness length of the surface.

B. The grain borne shear stress

In presence of saltating grains near the ground, the air can transfer momentum to the grains, which thereby transport a part of the shear stress down to the surface. This idea was introduced by Owen [4] and has widely been used in analytical saltation models and numerical simulations [5−7,11,12,21,22]. Accordingly, we distinguish the grain borne shear stress τ_g and the air borne shear stress τ_a, which together have to maintain the overall shear stress τ,

$$\tau=\tau_a(z)+\tau_g(z)=\text{const.} \tag{7}$$

At the top z_m of the saltation layer, the air borne shear stress τ_a has to be equal to the overall shear stress τ, $\tau_a(z_m)=\tau$.

The typical trajectory of a saltating grain intersects with each height level z two times, once when ascending and once when descending. Between these two intersections the wind accelerates the grain along its trajectory, thereby increasing its horizontal velocity between the ascending and descending intersection. From this velocity difference we can calculate the shear stress transported by the grains at each level z,

$$\tau_g(z)=\Phi[u_{down}(z)-u_{up}(z)]=\Phi\Delta u_g(z), \tag{8}$$

where Φ denotes the flux of grains impacting onto the surface, and u_{up} and u_{down} the horizontal velocity of the grains at the ascending and descending intersection of the trajectory with the height level z.

As sketched in Fig. 1 we can relate both the horizontal sand flux q and the flux of grains impacting onto the surface Φ to the number of grains N, their mass m, the saltation length l, and the flight T time for the trajectory,

$$\Phi=\frac{Nm}{laT}=\frac{q}{l}, \tag{9}$$

where a is the arbitrary width of the slice, considered here. Using Eqs. (8) and (9) the grain borne shear stress can be expressed by the horizontal flux of grains,

$$\tau_g(z)=\frac{q}{l}\Delta u_g(z). \tag{10}$$

In the following we restrict the discussion to the grain borne shear stress τ_{g0} at the ground that is given by the momentum transfer from the grains to the bed during their impacts as sketched in Fig. 1. We denote quantities that are taken at the ground with an index 0, e.g. $\tau_{g0}=\tau_g(z_0)$, where z_0 is the height at the ground. We need the impact and ejection velocities of the grains or moreover the change in horizontal velocity Δu_{g0} at the ground to calculate the momentum transfer. In order to keep the discussion simple we will directly formulate the model in terms of mean values for the trajectory length l and its time T instead of writing everything in terms of not well known distribution functions.

The average saltation length l and the average saltation time T are related by $l=u\,T$. We estimate both as the flight time and length of a simple ballistic trajectory,

$$T=\frac{2u_{z0}}{g}, \quad l=u\frac{2u_{z0}}{g}, \tag{11}$$

where u_{z0} is the vertical component of the initial velocity of the grain and g the acceleration by gravity. The typical values for the time and length of a mean saltation trajectory depend on the shear velocity u_*, $T(u_*)\approx 1.7\,u_*/g$ and $l(u_*)\approx 18\,u_*^2/g$ [14]. For a shear velocity $u_*=0.5\,\mathrm{m\,s^{-1}}$ we obtain $T\approx 0.08$ s and $l\approx 0.45$ m. Calculations of grain trajectories confirm that this approximation gives the correct order of magnitude for the flight time T, e.g., Sørensen obtained $T=1.75u_*/g$ [21]. Inserting the saltation length of Eq. (11) in Eq. (10) and using $q=\rho u$ we obtain

$$\tau_{g0}=\rho\frac{g}{2}\frac{\Delta u_{g0}}{u_{z0}}. \tag{12}$$

The relation between the impact and ejection velocity is in general defined by the splash function $S(u_{im}, \alpha_{im}, \ldots; u_{ej}, \alpha_{ej}, \ldots)$ giving the probability that a grain is ejected at a certain angle and velocity due to an impacting grain with a certain angle and velocity [11,14,15]. The simplest possibility is to take the vertical component of the ejection velocity u_{z0} proportional to the horizontal velocity difference Δu_{g0} and to neglect the angle dependence,

$$u_{z0}=\alpha\,\Delta u_{g0}. \tag{13}$$

Here, we have introduced the first model parameter α that represents an effective restitution coefficient for the grain-bed interaction. In principle, it can be calculated from the splash function S, but here we regard it as a phenomenological parameter to be determined later by comparing the model with experimental results. With Eq. (13), Eq. (12) reduces to the simple result

$$\tau_{g0} = \rho \frac{g}{2\alpha} \tag{14}$$

for the grain borne shear stress. The fact that it is linear in the density ρ and independent of the velocity u is an interesting result that is not *a priori* obvious. Indeed, if we had chosen the effective restitution coefficient $\alpha(u)$ as a function of the velocity we would obtain a velocity dependence. Why is the velocity unimportant or only of little importance for τ_{g0}? This can be explained by looking at the trajectory length of the saltating grains, which scales with the square of the horizontal velocity ($l \propto u^2$) leading to a decrease of the density of impacts with increasing u. This compensates the higher momentum transfer of a single grain due to its higher velocity.

C. Erosion and deposition rates

Grains impacting onto a bed of grains either rebounce directly or remain on the bed. In the latter case the energy of the impact can dislodge several new grains leading to a strong amplification of the grain density in the saltation layer and in turn to erosion. The probability that a certain number of grains leaves the surface with a certain velocity is in general given by the splash function S [11,14,15] mentioned above. A part of the information contained in the splash function has already been comprised into the model parameter α that relates the average horizontal velocity difference to the vertical component of the average ejection velocity. Another part can be represented by the average number n of grains disloged by an impacting grain. Together, α and n determine the simple effective splash function used in this model,

$$S(u_{z0}, \Delta u_{g0}) = n\,\delta(\alpha\,\Delta u_{g0} - u_{z0}). \tag{15}$$

Using the average number n of grains dislodged by an impacting grain we can define the erosion rate as the net average rate of grains leaving the surface, which is the difference between the flux of grains leaving the surface and the flux of grains impacting onto it,

$$\Gamma = \Phi(n-1) = \frac{\tau_{g0}}{\Delta u_{g0}}(n-1). \tag{16}$$

It is important to realize that the air borne shear stress within the saltation layer, and therewith n, is lowered if the number of grains in the saltation layer increases and vice versa. This is the feedback effect discussed in Sec. II. According to Owen [4], the air borne shear stress at the bed τ_{a0} in the equilibrium is just large enough to keep saltation alive and therefore close to the threshold $\tau_t = \rho_{air} u_{*t}^2$. For $\tau_{a0} > \tau_t$, the number of grains in the saltation layer increases in a chain reaction ($n > 1$) whereas for $\tau_{a0} < \tau_t$ ($n < 1$) saltation cannot be maintained. To model the average number n of dislodged grains out of equilibrium we write n as a function $n(\tau_a/\tau_t)$ with $n(1) = 1$. We furthermore assume that n can be expanded into a Taylor series at the threshold and neglect all terms after the linear order,

$$n\left(\frac{\tau_{a0}}{\tau_t}\right) = 1 + \tilde{\gamma}\left(\frac{\tau_{a0}}{\tau_t} - 1\right) \ldots . \tag{17}$$

The model parameter $\tilde{\gamma}$ characterizes the strength of the erosion and determines how fast the system reaches the equilibrium or reacts to perturbations. It depends on microscopic quantities and details of the grain-bed interaction, which are not available in the scope of this model. Therefore, we have to determine $\tilde{\gamma}$ later by comparison with measurements or microscopic computer simulations.

If we insert Eqs. (7) and (17) in Eq. (16), we obtain for the erosion rate

$$\Gamma = \tilde{\gamma} \frac{\tau_{g0}}{\Delta u_{g0}} \left(\frac{\tau - \tau_{g0}}{\tau_t} - 1 \right). \tag{18}$$

Assuming that the difference between impact and eject velocity of the grains is proportional to the mean grain velocity ($\Delta u_{g0} \propto u$) finally leads to

$$\Gamma = \gamma \frac{\tau_{g0}}{u} \left(\frac{\tau - \tau_{g0}}{\tau_t} - 1 \right), \tag{19}$$

where the proportionality constant is incorporated in γ. In order to close the system of equations we have to insert the expression for the grain borne shear stress τ_{g0} from Eq. (14).

Up to now, we discussed the entrainment of grains due to impacts of other grains, but if the air shear stress exceeds a certain value $\tau_{ta} > \tau_t$, called aerodynamic entrainment threshold, grains can directly be lifted from the bed. These directly entrained grains have been neglected up to now, because they are only important to initiate saltation [10,11]. Anderson [11] proposed an aerodynamic entrainment rate proportional to the difference between the air borne shear stress τ_a and the threshold τ_{ta},

$$\Gamma_a = \Phi_a \left(\frac{\tau_{a0}}{\tau_{ta}} - 1 \right) = \Phi_a \left(\frac{\tau - \tau_{g0}}{\tau_{ta}} - 1 \right), \tag{20}$$

where $\Phi_a \approx 5.7 \times 10^{-4}$ kg m^{-2} s^{-1} [11] is a model parameter defining the strength of the erosion rate for aerodynamic entrainment. This formula for the direct aerodynamic entrainment rate Γ_a has a similar structure as Eq. (19) for saltation induced entrainment, but the prefactors are different.

D. Forces

In Sec. III we introduced the drag and friction forces, f_{drag} and f_{bed}, acting on the saltation layer. In the following we have to specify these forces. Modeling the friction force is simple, because we already derived an expression for the grain borne shear stress at the ground τ_{g0}, Eq. (14). The bed friction f_{bed} has exactly to compensate this grain borne shear stress,

$$f_{bed} = -\tau_{g0}. \tag{21}$$

We represent the wind force acting on the grains inside the saltation layer by the Newton drag force

$$F_{drag}=\frac{1}{2}\rho_{air}C_d\frac{\pi d^2}{4}(v_{air}-v_g)|v_{air}-v_g| \tag{22}$$

of a spherical particle, where d denotes the grain diameter, C_d the drag coefficient, v_g the velocity of a grain, and v_{air} the velocity of the air. Multiplying F_{drag} with the density ρ of the saltation layer and dividing it by the mass m of a grain with diameter d and density ρ_{quartz}, we obtain the drag force acting on a volume element of the saltation layer,

$$f_{drag}=\rho\frac{3}{4}C_d\frac{\rho_{air}}{\rho_{quartz}}\frac{1}{d}(v_{eff}-u)|v_{eff}-u|. \tag{23}$$

Here, v_{eff} is an effective wind velocity, which is the wind speed taken at a reference height z_1 within the saltation layer. This reference height is another model parameter and has to be determined by comparing the sand flux with measured data as we will do it in Sec. IV. Neglecting the effect of the saltating grains on the wind field, we could use the logarithmic profile at z_1 to calculate the effective wind speed. But saltating grains in the air change the air shear stress and the wind speed. This is the feedback effect mentioned above and the mechanism how an equilibrium sand flux is reached. In order to calculate the perturbed wind speed we use again the standard turbulent closure (5), which relates the strain rate to the turbulent shear stress. In contrast to the case without grains, where the shear stress τ of the air is constant in z, the air borne shear stress τ_a as given by Eq. (7) is now varying in z,

$$\frac{\partial v}{\partial z}=\frac{u_*}{\kappa z}\sqrt{1-\frac{\tau_g(z)}{\tau}}. \tag{24}$$

The profile of $\tau_g(z)$ was found to be nearly exponential in simulations [11]. Furthermore, we already know the grain borne shear stress at the ground τ_{g0}. Hence, we can write

$$\frac{\partial v}{\partial z}=\frac{u_*}{\kappa z}\sqrt{1-\frac{\tau_{g0}}{\tau}e^{-z/z_m}}, \tag{25}$$

where z_m denotes the mean saltation height. The integration of Eq. (25) has to be performed from the roughness height z_0 to a reference height $z_1<z_m$. Therefore we linearize the exponential function to integrate Eq. (25) and obtain the effective wind velocity

$$v_{eff}=\frac{u_*}{\kappa}\sqrt{1-\frac{\tau_{g0}}{\tau}}\left(2A_1-2A_0+\ln\frac{(A_1-1)(A_0+1)}{(A_1+1)(A_0-1)}\right) \tag{26}$$

with

$$A_i=\sqrt{1+\frac{z_i}{z_m}\frac{\tau_{g0}}{\tau-\tau_{g0}}}. \tag{27}$$

For a reference height z_1 much smaller than the mean saltation height z_m ($z_0<z_1\ll z_m$) we can simplify Eq. (26) to

$$v_{eff}=\frac{u_*}{\kappa}\sqrt{1-\frac{\tau_{g0}}{\tau}}\left(2A_1-2+\ln\frac{z_1}{z_0}\right). \tag{28}$$

For vanishing grain borne shear stress $\tau_{g0}\to 0$, the effective wind velocity v_{eff} reduces to the velocity of the undisturbed logarithmic profile at height z_1. The values of the parameters z_0 and z_m can be obtained from measurements, whereas the value of the reference height z_1 is a free phenomenological parameter of the model that we have to estimate by comparing the saturated flux predicted by our model with measurements.

E. Closed model

So far, we have introduced the erosion rate Γ, the drag force f_{drag}, and the bed interaction f_{bed} and expressed them in the preceding sections in terms of the mean density ρ and the mean velocity u of the saltating grains. Furthermore, we have introduced two model parameters α and z_1 determining the equilibrium state of the saltation layer, and the parameter γ that controls the relaxation to equilibrium. Inserting Eqs. (19) and (14) in Eq. (1) leads to an equation for the sand density ρ in the saltation layer,

$$\frac{\partial\rho}{\partial t}+\frac{\partial}{\partial x}(\rho u)=\gamma\frac{g}{2\alpha}\frac{\tau-\tau_t}{\tau_t}\frac{\rho}{u}\left(1-\frac{g}{2\alpha}\frac{1}{\tau-\tau_t}\rho\right). \tag{29}$$

Here, we can identify two important physical quantities, the saturated density ρ_s and the characteristic time T_s that define the steady state and the transients of the sand density ρ, respectively,

$$\rho_s=\frac{2\alpha}{g}(\tau-\tau_t), \tag{30}$$

$$T_s=\frac{2\alpha u}{g}\frac{\tau_t}{\gamma(\tau-\tau_t)}. \tag{31}$$

With these expressions we can rewrite Eq. (29) in a more compact form,

$$\frac{\partial\rho}{\partial t}+\frac{\partial}{\partial x}(\rho u)=\frac{1}{T_s}\rho\left(1-\frac{\rho}{\rho_s}\right). \tag{32}$$

Direct aerodynamic entrainment, i.e., the initiation of saltation, has been neglected in Eq. (32), but can easily be included by adding the erosion rate Γ_a of Eq. (20) to the right hand side. Furthermore, inserting Eqs. (21) and (23) in Eq. (2) leads to a model for the sand velocity u in the saltation layer,

$$\frac{\partial u}{\partial t}+\left(u\frac{\partial}{\partial x}\right)u=\frac{3}{4}C_d\frac{\rho_{air}}{\rho_{quartz}}\frac{1}{d}(v_{eff}-u)|v_{eff}-u|-\frac{g}{2\alpha}, \tag{33}$$

with v_{eff} defined in Eq. (28). Finally, the Eqs. (32), (30), (31), (33), and (28) define the closed model for the sand flux in the saltation layer.

We want to emphasize that $T_s(\tau,u)$ and $l_s(\tau,u)=T_s u$ are not constant, but depend on the external shear stress τ of the

wind and the mean grain velocity u. Using Eq. (11) we can relate the characteristic time T_s and length l_s of the saturation transients to the saltation time T and the saltation length l of the average grain trajectory,

$$T_s = T\frac{\tau_t}{\tilde{\gamma}(\tau-\tau_t)}, \quad l_s = l\frac{\tau_t}{\tilde{\gamma}(\tau-\tau_t)}. \tag{34}$$

For typical wind speeds, the time to reach saturation is in the order of 2 s [10–12]. Assuming a grain velocity of 3–5 $\mathrm{m\,s^{-1}}$ [23] we obtain a length scale of the order of 10 m for saturation. This length scale is large enough to play an important role in dune formation. We want to emphasize that the characteristic length l_s and time T_s of the saturation transients, Eq. (34), naturally result from the saltation kinetics (in contrast to the heuristic ''adaptation length'' of Ref. [24]). Their functional dependence can be interpreted in the following way. The dominant mechanism to adapt the grain density in the saltation layer after a change in external conditions is by the chain reaction process modeled in Eq. (17). Hence, l_s and T_s depend inversely onto the ''stiffness'' $\tilde{\gamma}(\tau/\tau_t-1)$ of this multiplication process. Since the average grain can only influence the number of grains in the saltation layer at the discrete times and positions where it interacts with the bed, the saturation time/length are proportional to the time/length of the average trajectory. The resulting nontrivial dependence of the saturation kinetics on the external conditions, which may be appreciated from Fig. 5 in Sec. VI, is essential for a proper description of aeolian sand transport in structured terrain.

The mass and momentum Eqs. (32) and (33) are coupled partial differential equations and difficult to solve. In the following sections we will first discuss the fully saturated situation and later some dynamical properties of the saltation layer. Finally, we simplify the model in order to arrive at a minimal model that can easily be applied to geomorphological problems.

IV. SATURATED FLUX

The full dynamics of the saltation layer must be evaluated numerically, whereas the saturated flux — the stationary solution ($\partial/\partial t=0$) for a constant external shear stress [$\tau(x,t)=\tau$] and a homogeneous bed ($\partial/\partial x=0$) — can be calculated analytically from Eqs. (29) and (33). For shear velocities below the threshold ($u_*<u_{*t}$) the solution is trivial,

$$\rho_s(u_*)=0, \quad u_s(u_*)=0, \quad \text{and} \quad q_s(u_*)=0. \tag{35}$$

Above the threshold ($u_*>u_{*t}$) we obtain from Eq. (30) for the steady state density ρ_s,

$$\rho_s(u_*)=\frac{2\alpha\rho_{air}}{g}(u_*^2-u_{*t}^2). \tag{36}$$

Likewise we obtain from Eqs. (33) the steady state velocity u_s,

$$u_s(u_*)=\frac{2u_*}{\kappa}\sqrt{\frac{z_1}{z_m}+\left(1-\frac{z_1}{z_m}\right)\frac{u_{*t}^2}{u_*^2}}-\frac{2u_{*t}}{\kappa}+u_{st}, \tag{37}$$

where

$$u_{st}\equiv u_s(u_{*t})=\frac{u_{*t}}{\kappa}\ln\frac{z_1}{z_0}-\sqrt{\frac{2\,g\,d\,\rho_{quartz}}{3\,\alpha\,C_d\,\rho_{air}}} \tag{38}$$

is the minimum velocity of the grains in the saltation layer occurring at the threshold. In contrast to the density ρ_s the velocity u_s does not go continuously to zero near the threshold u_{*t}. This is intuitively obvious, because grains at the threshold have already a finite velocity u_{st}. Finally, we can write for the steady state flux $q_s=u_s\rho_s$,

$$q_s=2\alpha\frac{\rho_{air}}{g}(u_*^2-u_{*t}^2)\left[u_*\frac{2}{\kappa}\sqrt{\frac{z_1}{z_m}+\left(1-\frac{z_1}{z_m}\right)\frac{u_{*t}^2}{u_*^2}}-\frac{2u_{*t}}{\kappa}+u_{st}\right]. \tag{39}$$

For large wind speeds ($u_*\gg u_{*t}$) the flux is asymptotically proportional to u_*^3, which is in accord with the predictions of other saltation models [3,21,25].

The saturated flux q_s, given by Eq. (39), is now used to determine the model parameters α and z_1 by fitting it to flux data measured in a wind tunnel by White and Mounla [26]. Using the literature values: $g=9.81\ \mathrm{m\,s^{-2}}$, $\rho_{air}=1.225\ \mathrm{kg\,m^{-3}}$, $\rho_{quartz}=2650\ \mathrm{kg\,m^{-3}}$, $z_m=0.04\,\mathrm{m}$, $z_0=2.5\ 10^{-5}\,\mathrm{m}$, $D=d=250\,\mu\mathrm{m}$, $C_d=3$ and $u_{*t}=0.28\ \mathrm{m\,s^{-1}}$ [2,4,11] we obtain for the two model parameters $\alpha=0.35$ and $z_1=0.005\,\mathrm{m}$. For comparison we fitted to the same set of data the sand transport laws given by Bagnold [25],

$$q_B=C_B\frac{\rho_{air}}{g}\sqrt{\frac{d}{D}}u_*^3, \tag{40}$$

Lettau and Lettau [3],

$$q_L=C_L\frac{\rho_{air}}{g}u_*^2(u_*-u_{*t}), \tag{41}$$

and Sørensen [21],

$$q_S=C_S\frac{\rho_{air}}{g}u_*(u_*-u_{*t})(u_*+7.6^*u_{*t}+2.05\ \mathrm{m\,s^{-1}}) \tag{42}$$

and obtained $C_B=1.98$, $C_L=4.10$, and $C_S=0.48$.

The results are shown in Fig. 2, where the flux normalized by $q_0=\rho_{air}/(gu_*^3)$ is plotted versus the normalized shear velocity u_*/u_{*t}. Our result resembles Sørensen's equation but differs from the flux relation given by Lettau and Lettau. For high shear velocities all transport laws show a cubic dependence on the shear velocity.

The comparison of the saturated sand flux with experimental data determined the two phenomenological parameters α and z_1. As anticipated above, the value obtained for

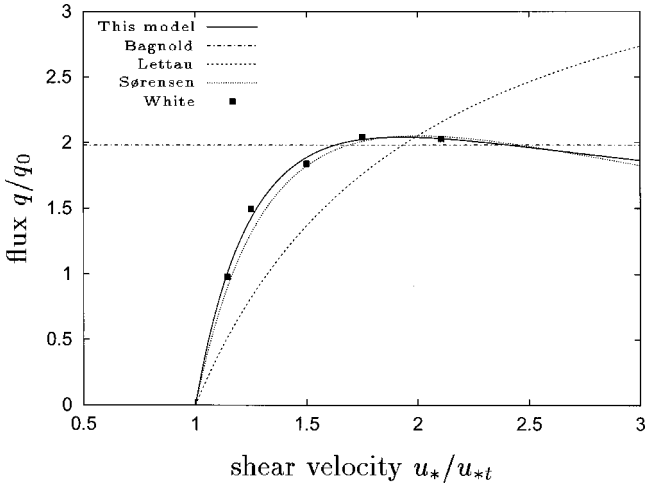

FIG. 2. Comparison of the different theoretical flux relations (39)–(42) fitted to wind tunnel data of White. The fluxes are normalized by $q_0=\rho_{air}/(gu_*^3)$. The saturated flux of our model and the relation of Sørensen reproduce quite well the data, whereas the others do not show the same structure.

z_1, the reference height for momentum transfer, is well below z_m, the mean height of the saltation trajectories. This justifies *a posteriori* the linearization in Eq. (25).

V. DYNAMICS

After the saturated case has been studied in the preceding section, we now investigate the dynamics of the saltation layer in order to get an estimate for the saturation time T_s and thus for the model parameter γ. Figure 3 shows numerical solutions of Eqs. (32) and (33) for the time evolution of the sand flux $q=u\,\rho$ using spatially homogeneous conditions $(\partial/\partial x=0)$. To get rid of the free parameters in Eq. (20) we neglected Γ_a, thus disregarding direct aerodynamic entrainment, and assumed instead a small initial density. Due to the multiplication effect of the saltation process, the flux increases first exponentially and reaches the equilibrium state

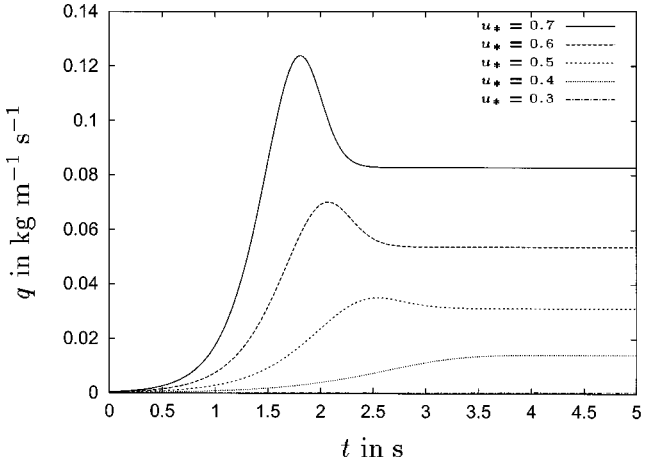

FIG. 3. Numerical simulations of the time evolution of the full model given by Eqs. (32) and (33) with a constant shear velocity u_*.

after passing through a maximum at $t\approx 2$ s. The time transients are controlled by the parameter γ and compare well with measurements by Butterfield [13] and microscopic simulations by Anderson [10,11] and McEwan and Willetts [12] for $\gamma\approx 0.4$. An important result of the simulations of Anderson was the dependence of the saturation time on the shear velocity and the overshoot near $t\approx 2$ s. Both features are well reproduced by our model.

VI. A MINIMAL MODEL FOR GEOMORPHOLOGICAL APPLICATIONS

The change of desert topographies, e.g., the movement, growth, and shrinkage of dunes, depends mainly on the sand transport or erosion and the perturbations of the wind field caused by the topographies themselves. Here, we restrict ourselves to the problem of the sand transport and assume that the shear velocity above a certain topography is known. The time evolution of the topography $h(x,t)$ is then given by the mass conservation,

$$\frac{\partial h}{\partial t}=-\frac{1}{\rho_{sand}}\frac{\partial q}{\partial x}, \tag{43}$$

where ρ_{sand} is the mean density of the immobile dune sand. To obtain the sand flux $q(x,t)$ one can in principle solve the coupled differential equations for the density ρ, Eq. (32), and velocity u, Eq. (33), of the sand in the saltation layer. However, for most geomorphological applications a simplified version of our model will be sufficient. In the following, we first derive this ''minimal model'' from the equations given in Sec. III E and then show its usefulness by discussing a particular practical application in Sec. VII.

The first simplification is to use the stationary solution $(\partial/\partial t=0)$ of Eqs. (32) and (33). This can be justified by the fact that there are several orders of magnitude between the time scale of saltation (approximately 2 s) and the time scale of the surface evolution of a dune (several days or weeks).

Next, we consider the convective term $(u\partial_x u)$ that is only important at places where large velocity gradients occur. This is for instance the case in the wake region behind the brink of a dune, where the wind speed at the ground decreases drastically due to the flow separation of the air. Here, the inertia of the grains becomes important. To solve the model for the deposition in a wake region we want to consider an idealized brink situation, where both the wind speed and the friction with the bed drop discontinuously from a finite value to zero. In this case, Eq. (33) reduces to

$$\frac{1}{2}\frac{\partial u^2}{\partial x}=\frac{3}{4}C_d\frac{\rho_{air}}{\rho_{quartz}}\frac{1}{d}u^2. \tag{44}$$

This predicts an exponential decrease of the grain velocity over a characteristic length scale $l_{dep}=4\,d\,\rho_{quartz}/(3\,C_d\,\rho_{air})\approx 0.25\,\mathrm{m}$. Hence, the deposition takes place within a length $l_{dep}\ll l_s$ much shorter than the saturation length l_s on the windward side. Field measurements of lee side deposition agree with this conclusion [27]. Outside the

wake regions, on the other hand, we can neglect the convective term $(u\partial_x u)$ and we obtain the mean stationary grain velocity from Eq. (33)

$$u(\rho)=v_{eff}(\rho)-\sqrt{\frac{2gd\rho_{quartz}}{3\alpha C_d\rho_{air}}}, \tag{45}$$

where $v_{eff}(\rho)$ is defined by Eqs. (28) and (14). Furthermore, near the threshold τ_t we can approximate $v_{eff}(\rho)$ by $v_{eff}(\rho_s)$ making only a negligible error. For high shear stresses this is not in general possible. But, the sand flux in macroscopic geomorphological applications is nearly everywhere saturated, apart from places where external variables change discontinously, e.g. at a phase boundary bedrock/sand or at a flow separation (see Fig. 7). Hence, we can replace the density ρ by the saturated density ρ_s for most applications, where the exact value of the flux at these places is not of importance. The advantage of this approximation is that the velocity u is decoupled from the density ρ and we can insert the saturated velocity u_s of Eq. (37) in Eq. (32). Rewriting Eq. (32) in in terms of the sand flux $q=\rho u_s$ and the saturated sand flux $q_s=\rho_s u_s$ of Eq. (39) leads to an equation for the sand flux q,

$$\frac{\partial}{\partial x}q=\frac{1}{l_s}q\left(1-\frac{q}{q_s}\right), \tag{46}$$

where

$$l_s=\frac{2\alpha}{\gamma}\frac{u_s^2}{g}\frac{\tau_t}{\tau-\tau_t} \tag{47}$$

is the saturation length depicted in Figure 5.

We want to emphasize that our most important result for geomorphological applications is Eq. (46), which extends a common saturated flux law by incorporating saturation transients. It is to some extent independent of the particular form of the functions l_s and q_s given in Eqs. (47) and (39). The latter can be regarded as additional predictions of our model that one could also replace by other phenomenological relations or data tables obtained from wind tunnel measurements if this turns out to be more suitable.

The saturated flux q_s (39) and the model parameters $\alpha=0.35$ and $z_1=0.005$ m have been discussed in Sec. IV and can be used unchanged in Eq. (46). But with respect to the full model of Sec. V the value of γ gets renormalized due to the simplifications made in order to obtain Eq. (46). The most obvious difference of the solution of Eq. (46), depicted in Fig. 4, compared to the result of the full model in Sec. V is the missing overshoot. The value of $\gamma=0.2$ had to be adapted in order to obtain saturation transients between 1 s and 2 s for typical values of u_*. The fact that the saturation length l_s increases for shear velocities near the threshold is unchanged and shown in Figs. 4 and 5.

VII. THE SAND FLUX ON THE WINDWARD SIDE OF A DUNE

The mass conservation, Eq. (43), and the saturated sand flux relation by Lettau and Lettau, Eq. (41), have been used many times to predict the evolution of a dune [9,28,29]. The most successful work was done by Wippermann and Gross [9], but even they obtained an unphysical deposition at the windward foot of the dune, which tended to stretch the dune in length and flatten it, finally. This was avoided by an *ad hoc* smoothing operation, which led to a numerically stable simulation by hiding the problem at the phase boundary (bedrock/sand). The boundary problem is evident for an isolated dune like a barchan sketched in Fig. 6. Recent field measurements [8] of the wind speed and the sand flux on the central slice of a barchan dune show a large discrepancy between the measured sand flux at the windward foot and the sand flux predicted by Eq. (41) for the measured wind speed. The measured sand flux was a monotonously increasing function, whereas the calculated sand fluxes decreased near the dune's foot due to the depression of the wind velocity. A decrease of the flux is correlated with deposition at the

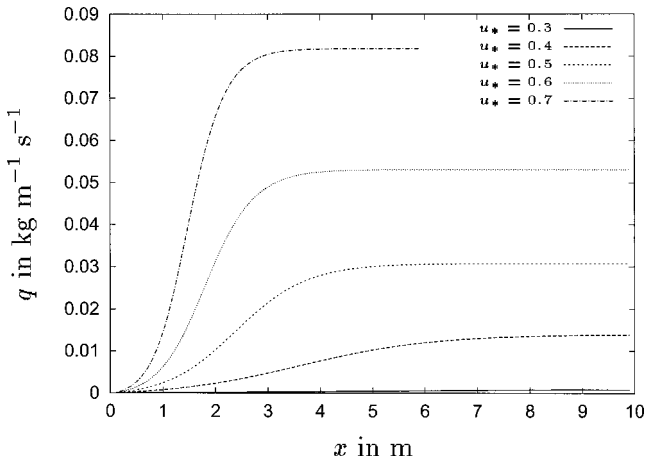

FIG. 4. Numerical solution of the sand flux equation (46) for different shear velocities u_*. The model parameter $\gamma=0.2$ that defines the length and time of the saturation transients was chosen here so that saturation is reached between 1 s and 2 s. Due to the simplifications made with respect to the full model, the initial overshoot is lost.

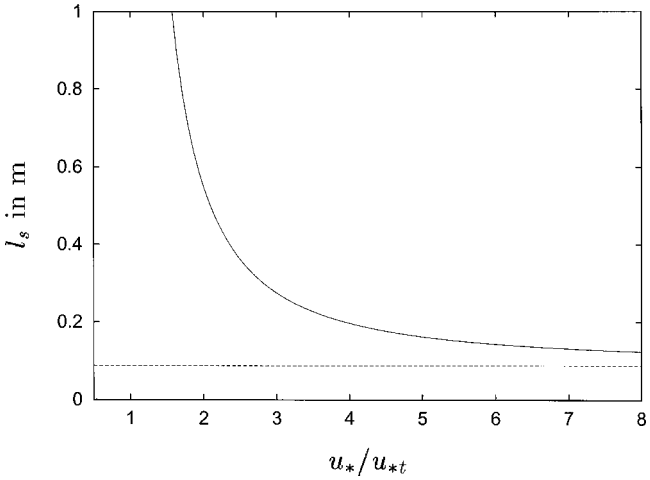

FIG. 5. The saturation length l_s from Eq. (47) is asymptotically constant for high shear velocities (horizontal line), but diverges for shear velocities near the threshold.

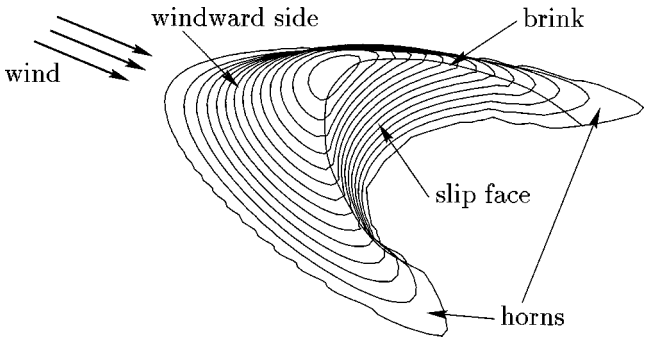

FIG. 6. Sketch of a barchan dune.

dune's foot leading to a flattening of the dune. Already from the measurements it is evident, that a saturated flux law cannot be applied near a phase boundary, where the bed changes suddenly from bedrock to sand. A further problem apears if we integrate Eq. (43) in time using a flux relation of the form $q(u_*)$ that determines the sand influx $q_{in}=q[u_*(x_{in})]$ and outflux $q_{out}=q[u_*(x_{out})]$ at the boundaries. This might be true for the outflux, but not for the influx, which depends normally on the upwind conditions and not on the wind speed at the boundary. In particular, the influx of an isolated dune in a dune field should depend on the outflux of several dunes upwind. Even situations without influx are possible, e.g., if there is vegetation around the dune.

To elucidate this problem further, we calculated the shear stress using FLUENT 5 [30] with a $k\epsilon$-turbulence model for the central profile, parallel to the wind direction, of a barchan measured in Morocco. (For more details see dune no. 7 in Ref. [31].) The exact calculation of the flow field is not of importance for the following discussion, which only relies on characteristic qualitative features such as the depression near the dune's foot. For the calculation of the sand flux we assume bedrock up to the dune's foot ($x_{in}=25$ m), where erosion is not possible ($q=$const). The sand flux over the bedrock is therefore equal to the influx at the boundary x_{in}. The sand flux q_L according to the relation by Lettau and Lettau, Eq. (41), and the solution of the saturated flux q_s, Eq. (39), predicted by our model are depicted in Fig. 7. Both models exhibit the unphysical deposition at the dune's foot described above. This problem is resolved, when the ''minimal model,'' Eqs. (46), (47), and (39), are applied. In contrast to a saturated flux law, the boundary conditions can freely be chosen in this model. Here, we used a constant influx q_{in}, much smaller than the saturated one, which represents the interdune sand flux. At the outflow boundary we applied $\partial q/\partial x=0$. The solution is plotted in Fig. 7 in comparison with the predictions of the simple flux relations. Due to the saturation transients we obtain a monotonously increasing flux and therefore no deposition of sand at the dune's foot. Finally, we want to point out that the flux on the entire windward side is never fully saturated due to the continuously increasing shear stress. However, away from the boundary it is always close to the saturated value (compare q and q_s in Fig. 7), which justifies the simplifications made in the ''minimal model.''

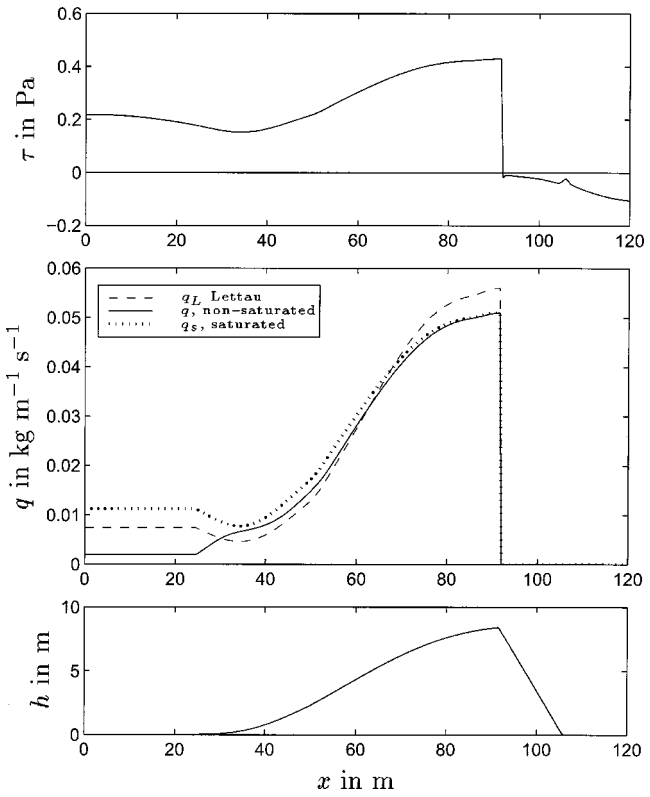

FIG. 7. Top: shear stress τ of the air at the surface, calculated by a $k\epsilon$-turbulence model using FLUENT 5. Center: The sand flux according to the ''minimal model,'' Eq. (46), the saturated sand flux q_s, Eq. (39), and the sand flux q_L predicted by the Lettau and Lettau relation (41) have been calculated using the shear stress depicted at the top. Bottom: Height profile of the symmetry plane of a barchan.

VIII. CONCLUSION AND OUTLOOK

We derived a phenomenological sand transport model that reproduces the equilibrium sand fluxes measured in wind tunnels. The predicted evolution of the sand flux with time has the same qualitative average behavior as the sand flux calculated with saltation models working on the microscopic grain scale. Finally, we proposed a ''minimal model'' that can be used as an efficient tool for geomorphological applications, such as the formation and migration of dunes. Furthermore, we showed that this model extends in a general way common saturated sand flux relation to a model that incorporates saturation transients.

The phenomenological parameters for the saltation model, which are effective restitution coefficients, a reference height within the saltation layer and a saturation length have been estimated by comparison with measurements.

Using these parameters we applied our model to a geomorphological problem and calculated the sand flux over a dune. We emphasized the importance of a nonequilibrium flux relation for the correct modeling of phase boundaries, e.g., bedrock/sand, as they naturally occur for isolated dunes. Furthermore, we have shown that the model predicts saturation transients to persist over the entire windward side of a

dune, where the shear stress increases from the foot to the brink. Therefore, we claim that the saturation length defines a length scale that is important for dune morphology in general. The investigation of the implications of saturation transients for dune formation are given in Ref. [32]. In particular, the question of shape differences between small and large dunes or the minimum size for slip-face formation are of interest and are discussed there. The extension of the model to three dimensions and inclined surfaces, which is necessary for applications to arbitrary terrains will be the subject of future work.

ACKNOWLEDGMENTS

We acknowledge the support of this work by the Deutsche Forschungsgemeinschaft (DFG) under Contract No. HE 2731/1-1. Furthermore, we thank J. Soares Andrade, Jr. for many fruitful discussions.

[1] R. A. Bagnold, Proc. R. Soc. London, Ser. A **157**, 594 (1936).
[2] K. Pye and H. Tsoar, *Aeolian Sand and Sand Dunes* (Unwin Hyman, London, 1990).
[3] K. Lettau and H. H. Lettau, *Exploring the World's Driest Climate*, edited by H. H. Lettau and K. Lettau (Center for Climatic Research, University of Wisconsin, Madison, 1978).
[4] P. R. Owen, J. Fluid Mech. **20**, 225 (1964).
[5] J. E. Ungar and P. K. Haff, Sedimentology **34**, 289 (1987).
[6] M. Sørensen, in Proceedings of International Workshop on Physics of Blown Sand, edited by O. E. Barndorff-Nielsen *et al.* (University of Aarhus, Aarhus, Denmark, 1985), Vol. 1, pp. 141–190.
[7] B. T. Werner, J. Geol. **98**, 1 (1990).
[8] G. F. S. Wiggs, I. Livingstone, and A. Warren, Geomorphology **17**, 29 (1996).
[9] F. K. Wippermann and G. Gross, Boundary-Layer Meteorol. **36**, 319 (1986).
[10] R. S. Anderson and P. K. Haff, Science **241**, 820 (1988).
[11] R. S. Anderson, Acta Mech., Suppl. 1, 21 (1991).
[12] I. K. McEwan and B. B. Willetts, Acta Mech., Suppl. 1, 53 (1991).
[13] G. R. Butterfield, in *Turbulence: Perspectives on Flow and Sediment Transport*, edited by N. J. Clifford, J. R. French, and J. Hardisty (Wiley, New York, 1993), Chap. 13, pp. 305–335.
[14] P. Nalpanis, J. C. R. Hunt, and C. F. Barrett, J. Fluid Mech. **251**, 661 (1993).
[15] F. Rioual, A. Valance, and D. Bideau, Phys. Rev. E **62**, 2450 (2000).
[16] J. P. Bouchaud, M. E. Cates, J. Ravi Prakash, and S. F. Edwards, J. Phys. I **4**, 1383 (1994).
[17] A. Mehta, J. M. Luck, and R. J. Needs, Phys. Rev. E **53**, 92 (1996).
[18] J. P. Bouchaud, in *Physics of Dry Granular Media*, Vol. 350 of NATO Advanced Studies Institute, Series B: Physics, edited by H. J. Herrmann, J-P. Hovi, and S. Luding (Kluwer Academic, Dordrecht, 1998).
[19] R. B. Hoyle and A. W. Woods, Phys. Rev. E **56**, 6861 (1997).
[20] R. B. Hoyle and A. Mehta, Phys. Rev. Lett. **83**, 5170 (1999).
[21] M. Sørensen, Acta Mech., Suppl. 1, 67 (1991).
[22] M. R. Raupach, Acta Mech., Suppl. 1, 83 (1991).
[23] B. B. Willetts and M. A. Rice, in Proceedings of the International Workshop on Physics of Blown Sand, edited by O. E. Barndorff-Nielsen (Memoirs, Denmark, 1985), Vol. 8, pp. 83–100.
[24] P. M. van Dijk, S. M. Arens, and J. H. van Boxel, Earth Surf. Processes Landforms **24**, 319 (1999).
[25] R. A. Bagnold, *The Physics of Blown Sand and Desert Dunes* (Methuen, London, 1941).
[26] B. R. White and H. Mounla, Acta Mech. **1,** Suppl. **1**, 145 (1991).
[27] R. R. McDonald and R. S. Anderson, Sedimentology **42**, 39 (1995).
[28] O. Zeman and N. O. Jensen, Risø National Laboratory Report No. M-2738, 1988.
[29] J. M. T. Stam, Sedimentology **44**, 127 (1997).
[30] Fluent Inc., FLUENT 5, 1999, finite volume solver.
[31] G. Sauermann, P. Rognon, A. Poliakov, and H. J. Herrmann, Geomorphology **36**, 47 (2000).
[32] K. Kroy, G. Sauermann, and H. J. Herrmann, e-print cond-mat/0101380.